



A Ta/W mixed addenda heteropolyacid with excellent acid catalytic activity and proton-conducting property

Shujun Li^a, Qingpo Peng^a, Xuenian Chen^{a,*}, Ruoya Wang^a, Jianxin Zhai^a, Weihua Hu^a, Fengji Ma^{b,*}, Jie Zhang^{a,*}, Shuxia Liu^c

^a School of Chemistry and Chemical Engineering, Henan Key Laboratory of Boron Chemistry and Advanced Energy Materials, Henan Normal University, Xinxiang, Henan 453007, China

^b College of Chemistry and Chemical Engineering, Anyang Normal University, Anyang, Henan 453000, China

^c Key Laboratory of Polyoxometalates Science of Ministry of Education, College of Chemistry, Northeast Normal University, Changchun City, Jilin 130024, PR China

ARTICLE INFO

Article history:

Received 9 June 2016

Received in revised form

31 July 2016

Accepted 1 August 2016

Available online 2 August 2016

Keywords:

Acid catalysis

Heteropolyacid

Ion-exchange

Proton conduction

Tantalum

ABSTRACT

A new HPAs $\text{H}_{20}[\text{P}_8\text{W}_{60}\text{Ta}_{12}(\text{H}_2\text{O})_4(\text{OH})_8\text{O}_{236}] \cdot 125\text{H}_2\text{O}$ (**H-1**) which comprises a Ta/W mixed addenda heteropolyanion, 20 protons, and 125 crystalline water molecules has been prepared through ion-exchange method. The structure and properties of **H-1** have been explored in detail. AC impedance measurements indicate that **H-1** is a good solid state proton conducting material at room temperature with a conductivity value of $7.2 \times 10^{-3} \text{ S cm}^{-1}$ (25 °C, 30% RH). Cyclic voltammograms of **H-1** indicate the electrocatalytic activity towards the reduction of nitrite. Hammett acidity constant H_0 of **H-1** in CH_3CN is -2.91 , which is the strongest among the present known HPAs. Relatively, **H-1** exhibits excellent catalytic activities toward acetal reaction.

© 2016 Elsevier Inc. All rights reserved.

1. Introduction

Heteropolyacids (HPAs) constitute a small but important subclass in Polyoxometalates (POMs) family, which are usually acidic forms of typical POMs [1,2]. Their heteropolyanions (anion clusters usually made up of W^{VI} or Mo^{VI} and oxygen) have lower basicity on the surface oxygen atoms, so they are strong Brønsted acids and have significantly higher catalytic activity than mineral acids, such as sulfonic acid and hydrochloric acid. In particular in organic media, the molar catalytic activity of HPA is often 100–1000 times higher than that of H_2SO_4 , and rarely leads to side reactions [3,4]. So, HPAs are highly suitable to catalyze various types of organic reactions in homogeneous liquid phase, and several processes with HPAs as the catalysts have been industrialized [1,5,6].

However, only limited HPAs with unambiguous structures determined by X-ray crystallography analysis or neutron diffraction analysis, including Keggin-type $\text{H}_3[\text{PW}_{12}\text{O}_{40}] \cdot n\text{H}_2\text{O}$ [7–9], and $\text{H}_3[\text{PMo}_{12}\text{O}_{40}] \cdot n\text{H}_2\text{O}$ [10], Dawson-type $\text{H}_7[\text{In}(\text{H}_2\text{O})\text{P}_2\text{W}_{17}\text{O}_{61}] \cdot 23\text{H}_2\text{O}$ [11] and sandwich complex $\text{H}_8[\text{Ti}_2\{\text{P}_2\text{W}_{15}\text{O}_{54}(\text{OH})_2\}_2] \cdot 31\text{H}_2\text{O}$ [12], have been reported owing to the following two

reasons. Firstly, most POMs compounds especially those with complex structures, are only stable under specific narrow pH ranges, and tend to convert into stable Keggin or Dawson species under strong acid conditions. Secondly, it is difficult to obtain single crystals of some HPAs suitable for X-ray diffraction measurements. Exploring novel type HPAs other than traditional Keggin or Dawson type is motivating for the farther development of HPAs and relevant acid catalysis areas.

On the other hand, although POMs based on V^{V} , Mo^{VI} , W^{VI} , and now even Nb^{V} provide frequent exciting advances, little is known about the POM chemistry of Ta^{V} [13]. The first polyoxotantalate ($\text{K}_8[\text{Ta}_6\text{O}_{19}]$) was discovered more than sixty years ago, but the synthesis of Ta-containing POMs is still challenging, mainly because the soluble Ta precursors (e.g. $[\text{Ta}_6\text{O}_{19}]^{8-}$ or TaCl_5) tend to form intractable gel-like materials or Ta_2O_5 precipitate in aqueous solution [14,15]. Recently our group and Nyman's group have demonstrated that it is feasible to access mixed metal Ta/W POMs in acidic solution [16,17]. These Ta/W mixed addenda POMs will provide excellent opportunity for the further development of Ta-POMs chemistry, because they exhibit unique property compared with the related Ta-POMs and W-POMs in term of electronic and electrochemical properties, solubility, stability, reactivity and photocatalytic performance. However, the research is still at the early stage, and only few examples of Ta/W mixed addenda compounds are known so far [18]. Much systematic and extended work still needs to do in this field.

* Corresponding author.

E-mail addresses: xnchen@htu.edu.cn (X. Chen), fengji.ma@yahoo.com (F. Ma), jie.zhang@htu.edu.cn (J. Zhang).

It has been demonstrated that Ta/W mixed addenda monomers have strong tendency to form aggregates by the formation of steady Ta–O–Ta bridges in acidic solution [17]. The very good stability of the polymerized Ta/W POMs in strong acid solution makes them promising for a new type of HPAs. In this report a full-acid (free-acid) form of tetrameric Ta/W mixed addenda POM $H_{20}[P_8W_{60}Ta_{12}(H_2O)_4(OH)_8O_{236}] \cdot 125H_2O$ (**H-1**) has been isolated as yellow crystals through ion-exchange method. The structure and properties of **H-1** have been discussed in detail. The acidity has been measured by UV–Vis spectrophotometry using a Hammett indicator. **H-1** exhibits excellent homogeneous acid catalytic activity and proton-conducting ability in solid state.

2. Experimental section

2.1. Materials and measurement

The precursor $K_8Na_8H_4[P_8W_{60}Ta_{12}(H_2O)_4(OH)_8O_{236}] \cdot 42H_2O$ (**1**) was synthesized according to the procedure described in the literature [17]. All other reagents were readily available from commercial sources and used without further purification. The FTIR spectra in KBr pellets were recorded in the range 400–4000 cm^{-1} with a VECTOR 22 Bruker spectrophotometer at room temperature. Elemental analyses for P, W, and Ta were determined with a PLASMASPEC (I) ICP atomic emission spectrometer. Powder X-ray diffraction (PXRD) measurements were performed on a Bruker D8 Advance Instrument with Cu $K\alpha$ radiation in the angular range $2\theta = 3\text{--}50^\circ$ at 293 K. The thermal behavior of **H-1** was examined by synchronousthermal analyses (TG/DSC, Netzsch 449 C Jupiter/QMS 403D). The samples were heated to 700 °C with a heating rate of 5 °C /min, under a flowing N_2 atmosphere. UV–Vis absorption spectra were obtained by using a UV-1700 UV–Vis spectrophotometer. The ^{31}P NMR spectra were measured on Avance-400 Bruker NMR spectrometers at an operating frequency of 16.66 MHz, with a 2.5 kHz sweep width, and 5-s pulse delay. Electrochemical measurements were performed with CHI1604E electrochemical workstation (Chenhua Instruments Co., Shanghai, China). Three-electrode system was employed in this study, a glass carbon electrode used as the working electrode, a Ag/AgCl electrode used as the reference electrode and a Pt coil used as the counter electrode. All the experiments were conducted at ambient temperature (20–25 °C).

2.2. Crystal structure determination

Single crystal XRD analysis of **H-1** was conducted on a Bruker Smart Apex CCD diffractometer with Mo $K\alpha$ monochromated radiation ($\lambda = 0.71073 \text{ \AA}$) at room temperature. The linear absorption coefficients, scattering factors for the atoms, and anomalous dispersion corrections were taken from the International Tables for X-Ray Crystallography [19]. Empirical absorption corrections were applied. The structures were solved by using the direct method and refined through the full matrix least-squares method on F^2 using SHELXS-97 [20]. Anisotropic thermal parameters were used to refine all non-hydrogen atoms. Those hydrogen atoms attached to lattice water molecules were not located. The crystal data and structure refinement results of **H-1** are summarized in Table 1. Further details on the crystal structure investigation scan be obtained free of charge from The Cambridge Crystallographic Data Centre via www.ccdc.cam.ac.uk/data_request/cif (depository number CCDC-1457311).

2.3. Proton conductivity measurement of H-1

Ac impedance spectroscopy measurement was performed on a chi660d (Shanghai chenhua) electrochemical impedance analyzer

Table 1
Crystal data and structural refinement for compound **H-1**.

Compound	H-1
Formula	$H_{20}[P_8W_{60}Ta_{12}(H_2O)_4(OH)_8O_{236}] \cdot 125H_2O$
Formula weight ($gmol^{-1}$)	18,729.56
T (K)	103 (2)
Wavelength (\AA)	0.71073
Crystal system	Tetragonal
Space group	P-421c
a (\AA)	24.185(2)
b (\AA)	24.185(2)
c (\AA)	27.067(3)
α ($^\circ$)	90
β ($^\circ$)	90
γ ($^\circ$)	90
$V(\text{\AA}^3)$	15,832(3)
Z	2
D_{calc} ($mg\ m^{-3}$)	3.929
μ (mm^{-1})	25.978
$F(000)$	16,152.0
Crystal dimensions mm^{-1}	$0.30 \times 0.26 \times 0.20$
Goodness-of-fit on F^2	0.907
Final R indices [$I > 2\sigma(I)$]	$R_1^a = 0.0855$, $wR_2^a = 0.1581$
R indices (all data)	$R_1^a = 0.1585$, $wR_2^a = 0.1942$

$$^a R_1 = \sum ||F_o| - |F_c|| / \sum |F_o|; wR_2 = (\sum [w(F_o^2 - F_c^2)^2] / \sum [w(F_o^2)^2])^{1/2}.$$

with copper electrodes (the purity of Cu is more than 99.8%) over the frequency range from 105 to 1 Hz. The powdered crystalline sample of **H-1** was compressed to 1.0–1.2 mm in thickness and 12.0 mm in diameter under a pressure of 12–14 MPa at room temperature. The conductivities were determined from the Nyquist plots. According to the Nyquist plot for **H-1** at each temperature and humidity, the proton conductivity was calculated as $\sigma = (1/R) (h/S)$, where R is the resistance, h is the thickness, and S is the area of the disk. The activation energy was calculated from the Arrhenius plot according to the formula $\sigma T = \sigma_0 \exp(-E_a/k_B T)$. Real (Z') and imaginary (Z'') parts of the impedance spectra are shown in Fig. 6 and Figs. S9–S10.

2.4. Acid strength measurement of H-1

Acidity measurements of **H-1** were performed in acetonitrile according to the procedure described in the literatures [21,22]. Diccinnamylideneacetone (pK_a value is -3.0 , where K_a is the dissociation constant of the protonated indicator $pK_a = -\log K_a$) was used as indicator. The concentration of Diccinnamylideneacetone and proton (based on the number of protons per HPAs) were set to $7 \times 10^{-4} \text{ mol/L}$ and $9.72 \times 10^{-4} \text{ mol/L}$ respectively. UV–vis absorption spectra were obtained by using a UV-1700 UV–Vis spectrophotometer. The Hammett acidity function (H_0) is defined by $H_0 = pK_a - \log[BH^+]/[B]$. $[BH^+]$ and $[B]$ are the concentrations of the protonated and neutral forms of the indicator in the equilibrium $BH^+ \rightleftharpoons B + H^+$. The ratio of the extinction coefficient of the two forms was estimated to be 1.3 by $H_3PW_{12}O_{40}$ (Fig. S11 and S12).

2.5. Preparation of $H_{20}[P_8W_{60}Ta_{12}(H_2O)_4(OH)_8O_{236}] \cdot 125H_2O$ (**H-1**)

400 mL 1 M HCl solution was poured into a column with an inner diameter of 15 mm charged with 100 g cationic exchange resin (Amberlite IR120B NA). A dripping rate of one drop/2 s was used. After that, the column was washed with deionized water to neutral.

3.0 g precursor (**1**) was dissolved in 5.0 mL deionized water, the resulting clear solution was passed through the above mentioned cation-exchange resin column at a dripping rate of one drop/2 s, then washed with deionized water to neutral. The collected solution was evaporated on a rotary evaporator at 80 °C, resulting in a

yellow solid of **H-1** with 94.7% yield (based on precursor **1**). Pure crystals product of **H-1** suitable for X-ray crystallography was obtained by recrystallization in water (2.66 g, 91.1% yield based on precursor **1**). Anal. Calcd (%) for **H-1**: P 1.26, Ta 11.02, W 55.98; found P 1.34, Ta 11.14, W 56.10. FTIR (KBr disk): 1091(s), 959(s), 903(sh), 773(vs), 562(w), 520(vw). ^{31}P NMR (ppm) – 11.21, – 14.13 in D_2O , and – 11.6, – 13.0 in CD_3CN .

3. Results and discussion

3.1. Synthesis and structure of H-1

The tetrameric Ta/W mixed addenda POM $\text{K}_8\text{Na}_8\text{H}_4[\text{P}_8\text{W}_{60}\text{Ta}_{12}(\text{H}_2\text{O})_4(\text{OH})_8\text{O}_{236}] \cdot 42\text{H}_2\text{O}$ (**1**), which consists of four lacunary Wells-Dawson $\{\text{P}_2\text{W}_{15}\text{O}_{56}\}$ segments linked by a central $\{\text{Ta}_{12}\}$ cluster and possesses remarkable photocatalytic H_2 evolution activity had been reported in our previous work [17]. Herein **H-1** was prepared by cationic ion exchange method using **1** as the precursor. Generally, HPAs can be prepared in aqueous solution and extracted with acidic diethyl ether, which is called the “etherate method”. But this method is fussy with low yield for **H-1** (shown in SI-1), by contrast, cationic ion exchange method described above is practical and simple.

H-1 possess the same space group (P-421c) and similar cell parameters with that of **1**. As shown in Figs. 1 and S1 the heteropolyanions packing in the cell form a body-centered tetragonal lattice in **H-1**. As conformed by X-ray crystallography analysis, acid base titration and TG analysis, there were 125 lattice water molecules and 20 H^+ ions in **H-1**. Abundant hydrogen bonds exist among the crystalline water molecules, the coordinated water molecules, and partial oxygen atoms of the polyanion. These hydrogen bonds extend around forming a three dimensional hydrogen bonding network (Figs. S2–S4), which is the potential channel for proton conduction. As found in other HPAs, the position of these protons cannot be determined directly by X-ray data, but may be delocalized among the hydrogen bonding network and polyanion, or combine with lattice water molecules forming hydrated ion (H_3O^+ , H_5O_2^+ , etc.) [1,23].

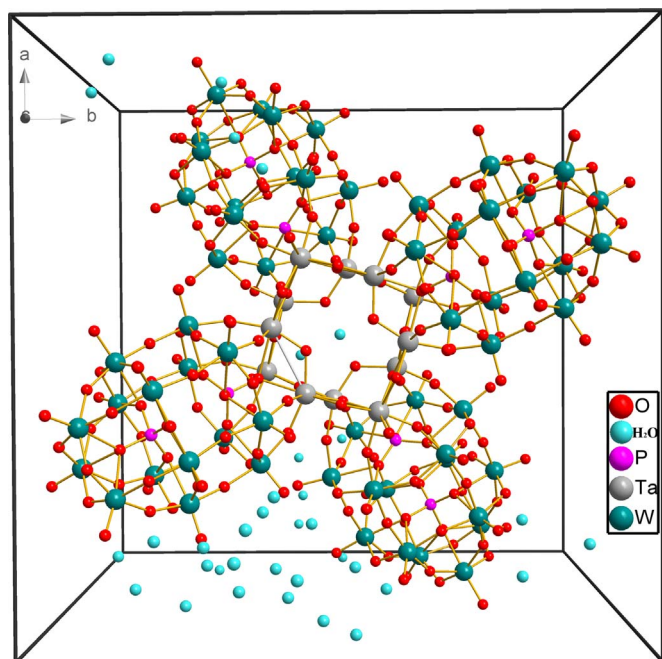


Fig. 1. Ball-and-stick representation of **H-1** in a unit cell, the aqua spheres represent lattice water molecular.

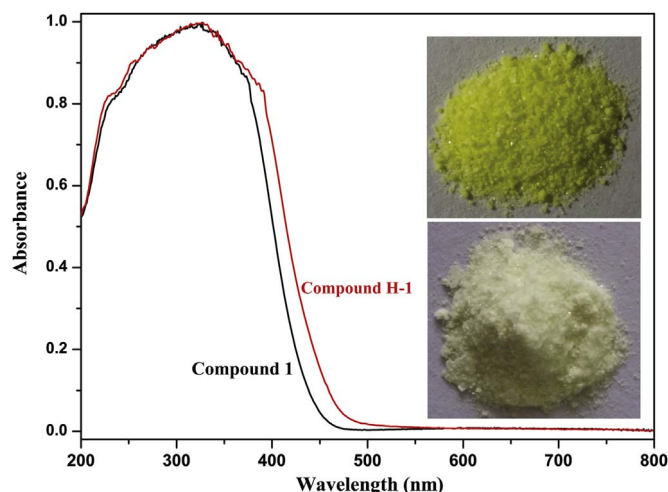


Fig. 2. The diffuse reflectance spectral of **H-1** (red line) and **1** (black line), and the digital photograph of **H-1** (top) and **1** (bottom). (For interpretation of the references to color in this figure legend, the reader is referred to the web version of this article.)

3.2. Solid properties

H-1 possesses similar cell parameters and appearance shape but different color with that of **1**. As shown in Fig. 2, **H-1** shows similar UV–vis diffuse reflectance spectra as that of **1**. The intense absorption bands in the range from 200 to 475 nm are mainly attributed to oxygen to metal ($\text{O} \rightarrow \text{M}$, $\text{M} = \text{W}^{6+}$ and Ta^{5+}) charge transfer (OMCT) transitions. The absorption edges of the yellow crystals of **H-1** shifted to a lower energy region compared with that of the colorless crystals of **1**. **H-1** shows similar PXRD patterns with **1** (Fig. S5). The calculated and experimental diffraction patterns of **H-1** match well, indicating that the bulk products obtained by cationic ion exchange method are homogeneous. The TG/DSC curve of **H-1** (Fig. S6) showed a total weight loss of 11.8% between 25 and 400 °C, which was attributed to the release of 125 lattice water molecules and four coordinated water molecules in the polyanion of **H-1**. Two exothermic peaks in the DSC curve above 580 °C were attributed to the decomposition of the polyanion skeletons in **H-1**. The FTIR spectra of **H-1** (Fig. S7) showed similar features to that of the precursor **1**, but the obvious shift for the bands arising from the $\text{M}-\text{O}_b$ and $\text{M}-\text{O}_t$ bonds ($\text{M} = \text{W}$ and Ta , O_b and O_t represent terminal oxygen atoms and bridging oxygen atoms) might be due to the strong interaction between protons and the polyanions.

3.3. Solution properties

The resulting yellow crystals of **H-1** are highly soluble in water, and soluble in organic solvent, such as acetone, methanol, ethanol, and acetonitrile, but insoluble in dichloromethane and chloroform.

To testify the solution stability of **H-1**, ^{31}P NMR spectra were taken in D_2O and CD_3CN respectively. The ^{31}P NMR spectra of **H-1** in D_2O showed two singlets at – 11.2 and – 14.1 ppm with 1:1 ratio (Fig. 3a), which is similar to that of the precursor **1** (– 11.4, – 14.4 ppm) [17]. The lower-field singlet at – 11.2 ppm was assigned to the P atom closest to the Ta side. Moreover, adjusting the pH of the solution from 0.1 to 6.0 by adding NaOH solution had no influence to the ^{31}P NMR spectra of **H-1**. **H-1** displayed similar ^{31}P NMR spectrum in CD_3CN (Fig. 3b), the higher-field signal of **H-1** shifted to a much lower field (– 13.0 ppm), whereas the lower-field singlet only little shifted to a higher field (– 11.6 ppm). Ta/W mixed addenda POM possess strong tendency to oligomerize under acidic conditions by the formation of stable Ta–O–Ta bonding motifs, therefore, **H-1** is extremely stable in both acid aqueous solution and organic solution. The UV/vis spectra of **H-1** in aqueous solution appear at 205.6 nm and 280.1 nm (Fig.

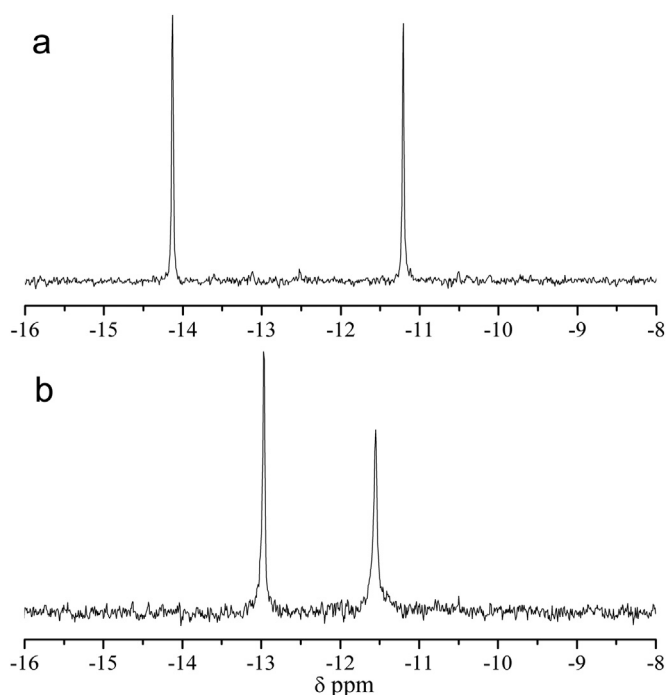


Fig. 3. ^{31}P NMR spectra of **H-1** in D_2O (a) and CD_3CN (b).

S8), corresponding to the charge transfer of $\text{O}_t\text{-W/Ta}$ and $\text{O}_{b/c}\text{-W/Ta}$ respectively [24].

3.4. Electrochemistry

The electrochemical behaviors of **H-1** were studied in 1.0 M NaAC + HAC (pH 4.7) aqueous solution at room temperature. The obtained cyclic voltammograms (CVs) of **H-1** at different scan rates are shown in Fig. 4a. **H-1** showed two reversible redox processes I-I', II-II' at $E_{1/2} = -914.5$ mV, -1072.5 mV arisen from the W centers [25]. Taking the anodic (I) and cathodic peak currents (I') as representative, at scan rates lower than 200 mV s^{-1} the peak currents increased linearly with the increase of the square root of scan rate, which indicates the redox process is limited by the diffusion of **H-1** to the electrode surface (Fig. 4b).

The electrocatalytic reduction of nitrate remains a challenge in the NO_x series because a complete process requires several electrons [26]. High nuclear POMs can serve as powerful electron

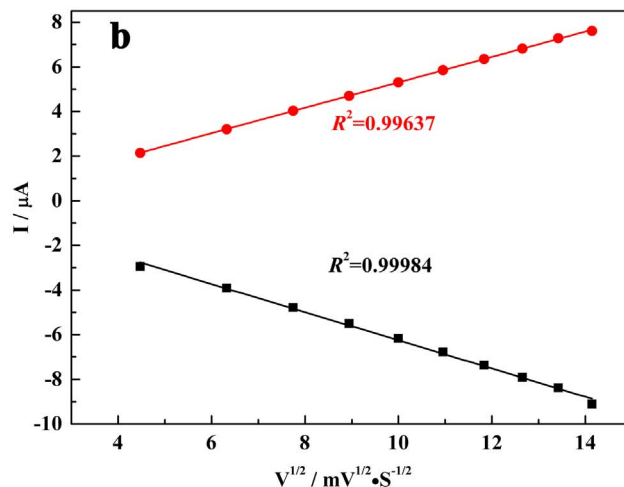
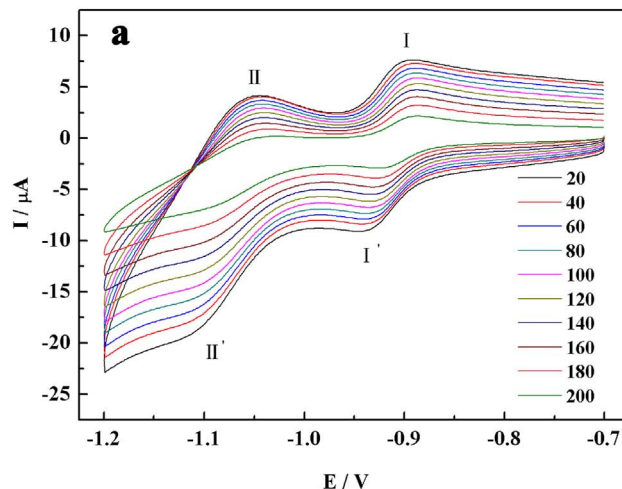


Fig. 4. a: Cyclic voltammogram of **H-1** in 1.0 M NaAC+HAC of pH=4.7 at different scan rates (from inner to outer: 20, 40, 60, 80, 100, 120, 140, 160, 180, 200 mV s^{-1}). b: The relationship of the scan rates vs the oxidation peak currents of I and reduction peak currents of I'.

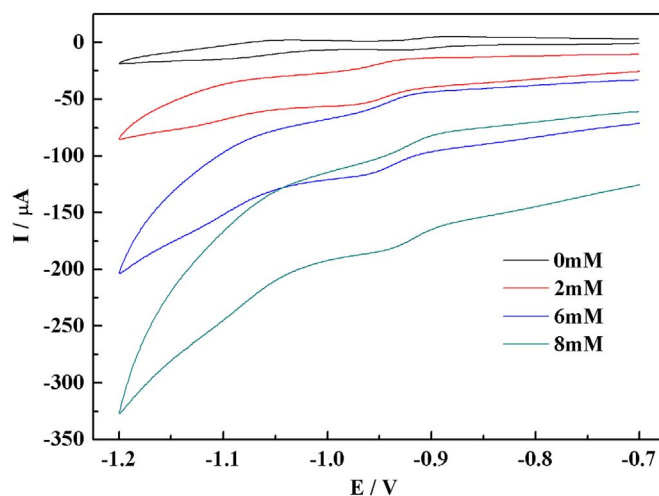


Fig. 5. Electrocatalysis reduction of NO_2^- in the presence of 1.0 mM **H-1** in a pH 4.7 medium (1.0 M NaAC+HAC), at a scan rate of 100 mV s^{-1} , containing NO_2^- concentrations of 0.0 mM (a), 2.0 mM (b), 6.0 mM (c), and 8.0 mM (d). The working electrode was glassy carbon and the reference electrode was Ag/AgCl.

reservoirs for multielectron reductions. The electron-enriched **H-1** is expected to have good catalytic activity. As shown in Fig. 5, with the addition of nitrite, all the reduction peak currents increase and the corresponding oxidation peak currents decrease dramatically, which indicates that the reduced species of the **H-1** show good electrocatalytic activities toward the reduction of nitrite.

3.5. Proton-conducting performance

AC impedance measurements indicated that **H-1** is good solid state proton conducting materials at room temperature and even at low humidity. At room temperature (25 $^\circ\text{C}$) and 30% relative humidity (RH), the conductivity value of **H-1** is 7.2×10^{-3} S cm^{-1} , which is superior to most POMs compounds reported recently [27–29], and comparable with the Dawson-type vanadium substituted HPAs $\text{H}_9\text{P}_2\text{W}_{15}\text{V}_3\text{O}_{62} \cdot 28\text{H}_2\text{O}$ [30]. With the increase of RH, the conductivity of **H-1** at 25 $^\circ\text{C}$ is gradually enhanced, and reaches to 5.0×10^{-2} S cm^{-1} at 98% RH (Fig. S9).

To account for the temperature influence in proton conduction, the conductivity of **H-1** at different temperature (30, 45, 60, 75 and 95 $^\circ\text{C}$, Fig. S10) was also studied under 30% RH. As shown in the

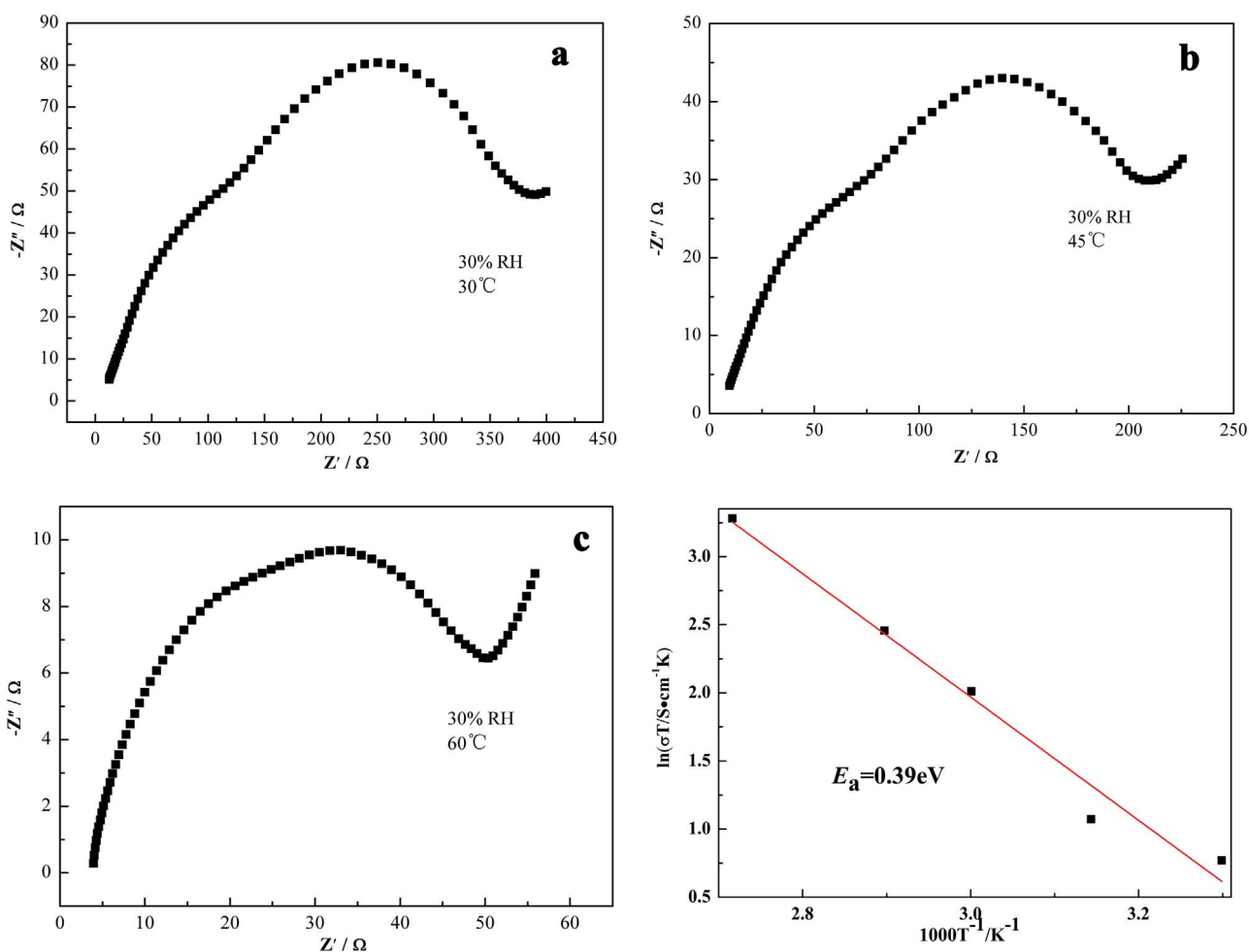


Fig. 6. Nyquist plots of proton conduction for **H-1** at 30 °C (a), 45 °C (b), and 60 °C (c) under 30% RH. And the Arrhenius plot of proton conductivity of **H-1** (d).

black line of Fig. 6, the conductivity of **H-1** increases with the increasing of temperature: $7.1 \times 10^{-3} \text{ S cm}^{-1}$ at 30 °C (Fig. 6a), $2.2 \times 10^{-2} \text{ S cm}^{-1}$ at 60 °C (Fig. 6b) and $7.2 \times 10^{-2} \text{ S cm}^{-1}$ at 95 °C (Fig. 6c). Proton transition within the hydrogen bonding network of **H-1** may be accelerated at higher temperature, thus increase the conductivity. The activation energy calculated from the Arrhenius plot is 0.39 eV (Fig. 6d), suggesting that Grotthuss mechanism is dominant in the proton transfer [31]. This result is consistent with the existence of abundant hydrogen bonds and the hydrogen bonding network in **H-1**. Solid HPAs usually contain abundant lattice water molecules, among which hydrogen-bond networks for proton conducting can form. Moreover, solid HPAs possess extremely high proton mobility, so can serve as promising solid state proton conducting materials [32]. There are 125 lattice water molecular and 20 H^+ in **H-1**. Moreover, abundant hydrogen bonds exist among the crystalline water molecules, the coordinated water molecules, and partial oxygen atoms of the polyanion (Figs. S2–S4). These hydrogen bonds extend around to make a three dimensional hydrogen bonding network in **H-1**, which is the potential channel and may be the main cause for proton conduction. Furthermore, the structure type and large size of the Ta/W mixed addenda polyanion of **H-1** may also contributive to the excellent conductivity. This inspires us to find more mixed addenda HPAs with different structures and sizes and investigate their proton-conducting performance, by which searching for a general structure-function relationship.

3.6. Acidity and acid catalysis

Acidity measurements of **H-1** were performed according to the procedure described in the literature and the detailed results are shown in SI-5 [33]. Generally, the acidity of HPAs of the same structure decreases as the number of protons increase, for example, the acidity of Keggin-type HPAs: $\text{H}_3\text{PW}_{12}\text{O}_{40} > \text{H}_4\text{SiW}_{12}\text{O}_{40} > \text{H}_4\text{GeW}_{12}\text{O}_{40} > \text{H}_5\text{BW}_{12}\text{O}_{40}$. The acidity of known Dawson HPAs series are relatively higher than that of Keggin series, for example, the Hammett acidity constant H_0 of $\text{H}_3\text{PW}_{12}\text{O}_{40}$ and $\text{H}_6\text{P}_2\text{W}_{18}\text{O}_{62}$ are -2.14 and -2.77 respectively [12,34]. Unfortunately, HPAs and acidity with novel structures other than classical Keggin or Dawson types are scarce reported. The Hammett acidity constant H_0 of **H-1** in CH_3CN , using dicinnamalacetone as Hammettin dicator is -2.91 , which is the strongest among present known HPAs (shown in Table 2).

To evaluate the acid catalytic properties of **H-1**, acetal reaction between benzaldehyde and five types of alcohols were investigated; the results are listed in Table 3. Compared with other reported HPAs [34,35], **H-1** showed significantly higher catalytic activity for the reactions involving methyl alcohol, ethyl alcohol, isopropanol and ethanediol. The reaction conversion involving methyl alcohol, n-butyl alcohol and ethanediol were higher than 80%. But ethyl alcohol, 2-butyl alcohol, and tertiary butanol provided relatively low conversion.

The reaction of benzaldehyde and ethanediol was chosen to compare the catalytic activity of **H-1** with other HPAs. As shown in

Table 2
Acidity of HPAs obtained from UV–vis spectra with Hammettin dicator.

HPAs	-H ₀
H-1	2.91
H ₆ P ₂ W ₁₈ O ₆₂	2.77 [12]
H ₄ S ₂ W ₁₈ O ₆₂	2.70 [31]
H ₈ [Ti ₂ {P ₂ W ₁₅ O ₅₄ (OH ₂) ₂ }] ₂ ·31H ₂ O	2.72 [12]
H ₃ PW ₁₂ O ₄₀	2.14 [29]/2.13 ^a
H ₄ SiW ₁₂ O ₄₀	1.98 [34]
H ₅ BW ₁₂ O ₄₀	1.55 [34]

^a Tested value in our experiments.

Table 4
The reactions of benzaldehyde and ethanediol catalyzed by different HPAs.^a

HPAs	Conversion (%)	TON ^b	TOF (h ⁻¹) ^c
1-A	83.5	4810	1603
1	9.2	527	176
H ₆ [P ₂ W ₁₈ O ₆₂]	32.9	1900	633
H ₃ [PW ₁₂ O ₄₀]	26.9	1552	517

^a Reaction conditions: benzaldehyde 3.3 mmol, ethanediol 25 mmol, HPAs 0.17 mol%, room temperature, 3 h.

^b TON = mol of product/mol of HPAs.

^c TOF = mol of product/(mol of HPAs · time (h))

negative charge may endow the protons relatively independent. This may be the primary cause for the stronger acidity and acid catalytic activity of **H-1** comparing with other traditional HPAs.

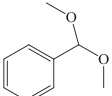
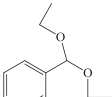
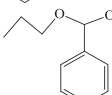
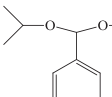
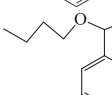
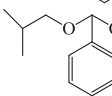
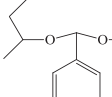
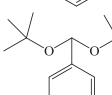
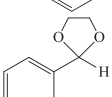
4. Conclusion

A new HPAs (**H-1**) which comprises a Ta/W mixed addenda heteropolyanion [P₈W₆₀Ta₁₂(H₂O)₄(OH)₈O₂₃₆]²⁰⁻, 20 protons, and

Table 4, at room temperature, **H-1** showed a significantly higher catalytic activity than the traditional HPAs H₆[P₂W₁₈O₆₂], H₃[PW₁₂O₄₀], and H₄[SiW₁₂O₄₀] (32% yield at room temperature, 24 h) [35].

It had been demonstrated that the catalytic activity was correlated with both the strong Brønsted acid strength and the softness of the anion in homogeneous Heteropolyacid system [35,36]. The softness of the polyanions in **H-1** resulting from the large size and large

Table 3
Acetal reactions of benzaldehyde and different alcohols with **H-1** as catalyst.^a

Entry	Reagent	Product	Conversion (%)	TON ^b	TOF (h ⁻¹) ^c
1	Methyl alcohol		84	4828	3218
2	Ethyl alcohol		37	2126	1418
3	Propyl alcohol		77	4425	2950
4	Isopropanol		59	3391	2261
5	n-Butyl alcohol		81	4655	3103
6	Isobutanol		75	4310	2874
7	2-Butyl alcohol		29	1667	1111
8	Tertiary butanol		25	1437	958
9	Ethanediol		83	4770	3180

^a Reaction conditions: benzaldehyde 3.3 mmol, alcohol 25 mmol, **H-1** 10 mg, 90 min. The reaction temperatures are 100 °C for entry 5 and 9, and refluxing temperatures for entry 1, 2, 3, 4, 6, 7, and 8.

^b TON = mol of product/mol of HPAs.

^c TOF = mol of product/(mol of HPAs · time (h))

125 crystalline water molecules has been prepared and re-presented. AC impedance measurements indicate that **H-1** is a good solid state proton conducting materials at room temperature with conductivity value of $7.2 \times 10^{-3} \text{ S cm}^{-1}$ (25 °C, 30% RH). Hammett acidity constant H_0 of **H-1** in CH_3CN is -2.91 , which is the strongest among present known HPAs. Relatively, **H-1** exhibits excellent catalytic activities toward acetal reaction. The present work offers a new approach to the development of novel HPAs, and indicates that Ta/W mixed addenda HPAs are a potential subclass of acid catalysts. Our future work will be extended to exploring more Ta/W or Nb/W mixed addenda HPAs and relevant acid catalysis studies.

Acknowledgments

This work was supported by the National Natural Science Foundation of China (Grant nos. 21401047, 21301010, and 21371051), Science and Technology Key Project of Education Department of Henan Province (Grant no. 14A150019).

Appendix A. Supplementary material

Supplementary data associated with this article can be found in the online version at doi:10.1016/j.jssc.2016.08.003.

References

- [1] I.V. Kozhevnikov, *Chem. Rev.* 98 (1998) 171–198.
- [2] M.S.S. Balula, I.C.M.S. Santos, M.M.Q. Simões, M.G.P.M.S. Neves, J.A.S. Cavaleiro, A.M.V. Cavaleiro, *J. Mol. Catal. A: Chemical* 222 (2004) 159.
- [3] D. Sloboda-Rozner, P. Witte, P.L. Alsters, R. Neumann, *Adv. Synth. Catal.* 346 (2004) 339.
- [4] A. Rezaeifard, R. Haddad, M. Jafarpour, M. Hakimi, *J. Am. Chem. Soc.* 135 (2013) 10036.
- [5] M. Misono, *Catal. Today* 144 (2009) 285–291.
- [6] A. Haimov, R. Neumann, *J. Am. Chem. Soc.* 128 (2006) 15697.
- [7] Y. Kikukawa, S. Yamaguchi, K. Tsuchida, Y. Nakagawa, K. Uehara, K. Yamaguchi, N. Mizuno, *J. Am. Chem. Soc.* 130 (2008) 5472.
- [8] S. Pathan, A. Patel, *Dalton Trans.* 42 (2013) 11600.
- [9] S. Shinachi, M. Matsushita, K. Yamaguchi, N. Mizuno, *J. Catal.* 233 (2005) 81.
- [10] Y. Kikukawa, S. Yamaguchi, Y. Nakagawa, K. Uehara, S. Uchida, K. Yamaguchi, N. Mizuno, *J. Am. Chem. Soc.* 130 (2008) 15872.
- [11] X. Qian, X. Tong, Q. Wu, Z. He, F. Cao, W. Yan, *Dalton Trans.* 41 (2012) 9897–9900.
- [12] H. Murakami, K. Hayashi, I. Tsukada, T. Hasegawa, S. Yoshida, R. Miyano, C. N. Kato, K. Nomiya, *Bull. Chem. Soc. Jpn.* 80 (2007) 2161–2169.
- [13] L.B. Fullmer, P.I. Molina, M.R. Antonio, M. Nyman, *Dalton Trans.* 43 (2014) 15295–15299.
- [14] W.H. Nelson, R.S. Tobias, *Inorg. Chem.* 2 (1963) 985–992.
- [15] M. Nyman, P.C. Burns, *Chem. Soc. Rev.* 41 (2012) 7354–7367.
- [16] I. Boldini, G. Guillemot, A. Caselli, A. Proust, E. Gallo, *Adv. Synth. Catal.* 352 (2010) 2365.
- [17] S. Li, S. Liu, S. Liu, Y. Liu, Q. Tang, Z. Shi, S. Ouyang, J. Ye, *J. Am. Chem. Soc.* 134 (2012) 19716–19721.
- [18] S.-Q. Shi, Y.-G. Chen, J. Gong, Z.-M. Dai, L.-Y. Qu, *Transit. Met. Chem.* 30 (2005) 136–140.
- [19] N.F.M. Henry, K. Lonsdale (Eds.), *International Tables for X-ray Crystallography*, Kynoch Press, Birmingham, 1952.
- [20] G.M. Sheldrick, *SHELXS-97: Programs for Crystal Structure Solution*, University of Göttingen, Göttingen Germany, 1997.
- [21] T. Okuhara, C. Hu, M. Hashimoto, M. Misono, *Bull. Chem. Soc. Jpn.* 67 (1994) 1186–1188.
- [22] T. Ueda, K. Yamashita, A. Onda, *Appl. Catal. A* 485 (2014) 181–187.
- [23] G.J. Kearley, H.A. Pressman, R.C.T. Slade, *J. Chem. Soc. Chem. Commun.* (1986) 1801–1802.
- [24] C. Tan, b. W. Bu, *J. Solid State Chem.* 219 (2014) 93–98.
- [25] X.-L. Wang, Z.-H. Chang, H.-Y. Lin, G.-C. Liu, C. Xu, J. Luan, A.-X. Tian, J.-W. Zhang, *Inorg. Chim. Acta* 443 (2014) 16–22.
- [26] F. Dhifallah, M.S. Belkhiria, N. Leclerc, E. Cadot, *Inorg. Chim. Acta* 441 (2016) 15–19.
- [27] C. Dey, T. Kundu, H.B. Aiyappa, R. Banerjee, *RSC Adv.* 5 (2015) 2333–2337.
- [28] G.-J. Cao, J.-D. Liu, T.-T. Zhuang, X.-H. Cai, S.-T. Zheng, *Chem. Commun.* 51 (2015) 2048–2051.
- [29] C. Dey, T. Kundu, R. Banerjee, *Chem. Commun.* 48 (2012) 266–268.
- [30] X. Tong, X. Wu, Q. Wu, W. Zhu, F. Cao, W. Yan, *Dalton Trans.* 41 (2012) 9893–9896.
- [31] K.-D. Kreuer, *Proton conductivity: materials and applications*, *Chem. Mater.* 8 (1996) 610–641.
- [32] Y. Zhou, J. Yang, H. Su, J. Zeng, S.P. Jiang, W.A. Goddard, *J. Am. Chem. Soc.* 136 (2014) 4954–4964.
- [33] T. Okuhara, C. Hu, M. Hashimoto, M. Misono, *Bull. Chem. Soc. Jpn.* 67 (1994) 1186–1188.
- [34] T. Ueda, K. Yamashita, A. Onda, *Appl. Catal. A* 485 (2014) 181–187.
- [35] S. Sato, K. Sagara, H. Furuta, F. Nozaki, *J. Mol. Catal. A: Chemical* 114 (1996) 209–216.
- [36] S. Wang, G. Yang, *Chem. Rev.* 115 (2015) 4893–4962.